# Role of Hydrogen Bonds in the Reaction Mechanism of Chalcone Isomerase†

Joseph M. Jez,‡ Marianne E. Bowman, and Joseph P. Noel*

*Structural Biology Laboratory, The Salk Institute for Biological Studies, 10010 North Torrey Pines Road, La Jolla, California 92037*

*Received January 9, 2002; Revised Manuscript Received February 21, 2002*

ABSTRACT: In flavonoid, isoflavonoid, and anthocyanin biosynthesis, chalcone isomerase (CHI) catalyzes the intramolecular cyclization of chalcones into (*S*)-flavanones with a second-order rate constant that approaches the diffusion-controlled limit. The three-dimensional structures of alfalfa CHI complexed with different flavanones indicate that two sets of hydrogen bonds may possess critical roles in catalysis. The first set of interactions includes two conserved amino acids (Thr48 and Tyr106) that mediate a hydrogen bond network with two active site water molecules. The second set of hydrogen bonds occurs between the flavanone 7-hydroxyl group and two active site residues (Asn113 and Thr190). Comparison of the steady-state kinetic parameters of wild-type and mutant CHIs demonstrates that efficient cyclization of various chalcones into their respective flavanones requires both sets of contacts. For example, the T48A, T48S, Y106F, N113A, and T190A mutants exhibit 1550-, 3-, 30-, 7-, and 6-fold reductions in $k_{cat}$ and 2−3-fold changes in $K_m$ with 4,2′,4′-trihydroxychalcone as a substrate. Kinetic comparisons of the pH-dependence of the reactions catalyzed by wild-type and mutant enzymes indicate that the active site hydrogen bonds contributed by these four residues do not significantly alter the p$K_a$ of the intramolecular cyclization reaction. Determinations of solvent kinetic isotope and solvent viscosity effects for wild-type and mutant enzymes reveal a change from a diffusion-controlled reaction to one limited by chemistry in the T48A and Y106F mutants. The X-ray crystal structures of the T48A and Y106F mutants support the assertion that the observed kinetic effects result from the loss of key hydrogen bonds at the CHI active site. Our results are consistent with a reaction mechanism for CHI in which Thr48 polarizes the ketone of the substrate and Tyr106 stabilizes a key catalytic water molecule. Hydrogen bonds contributed by Asn113 and Thr190 provide additional stabilization in the transition state. Conservation of these residues in CHIs from other plant species implies a common reaction mechanism for enzyme-catalyzed flavanone formation in all plants.

Flavonoids are versatile secondary metabolites used by plants for protection against UV light, as floral pigments for attracting pollinators, as inducers of *Rhizobium* nodulation genes, and as potent anti-microbial compounds produced in response to pathogen infestations (*1*). Moreover, many flavonoids and related compounds serve as important micronutrients with potent disease-preventing activities in human diets rich in plant-derived foodstuffs (*2*). Given the agricultural and health-promoting roles of flavonoids, there is considerable interest in understanding and manipulating the biosynthesis of these compounds. For example, recent introduction of the petunia *CHI* gene into tomato resulted in fruits with increased flavonol content (*3*). By examining the enzymes involved in flavonoid biosynthesis using structural and mechanistic studies, new opportunities arise for metabolic engineering of these biosynthetic pathways (*4*).

In flavonoid biosynthesis, chalcone isomerase (CHI, EC 5.5.1.6)[1] catalyzes the intramolecular cyclization of chalcones into (*2S*)-flavanones (Figure 1A) (*5*, *6*). The three-dimensional structures of *Medicago sativa* (alfalfa) CHI alone and complexed with different flavanones (Figure 1B) explain how the enzyme controls the stereochemistry of the cyclization reaction and suggest a likely catalytic mechanism (*7*, *8*). In the proposed reaction mechanism, the 2′-oxyanion forms spontaneously in solution. Once bound by CHI, the 2′-oxyanion is positioned for a stereochemically defined Michael addition to the α,β-unsaturated double bond of chalcone substrates; meanwhile a water molecule situated at the bottom of the active site acts as the general acid during transient protonation of the enolate intermediate. Mechanistic studies examining the pH-dependence of the cyclization reaction demonstrate that deprotonation of the chalcone 2′-hydroxyl group is facile at physiologic pH and that CHI-catalyzed flavanone formation occurs in a diffusion-limited reaction (*8*). These studies suggest that CHI accelerates the

† This work was supported by a grant from the National Science Foundation (MCB9982586) to J.P.N. J.M.J. was an NIH Postdoctoral Research Fellow (CA80396).

* To whom correspondence should be addressed at The Salk Institute for Biological Studies. Phone: (858) 453-4100, ext. 1442. Fax: (858) 452-3683. E-mail: noel@sbl.salk.edu.

‡ Current address: Kosan Biosciences, Inc., 3832 Bay Center Place, Hayward, CA 94545.

[1] Abbreviations: chalcone, 4,2′,4′,6′-tetrahydroxychalcone; CHI, chalcone isomerase (EC 5.5.1.6); 6′-deoxychalcone, 4,2′,4′-trihydroxychalcone; 4′-hydroxyflavanone, 2-(4-hydroxy-phenyl)-chroman-4-one; 7,4′-dihydroxyflavanone, 7-hydroxy-2-(4-hydroxy-phenyl)-chroman-4-one; 7-hydroxyflavanone, 7-hydroxy-2-phenyl-1-chroman-4-one; HEPES, 4-(2-hydroxyethyl)-1-piperazine-ethanesulfonic acid; naringenin, 5,7,4′-trihydroxyflavanone; NTA, nitrilotriacetic acid; PCR, polymerase chain reaction; SSRL, Stanford Synchrotron Radiation Laboratory; TRIS-HCl, tris(hydroxymethyl)-aminomethane hydrochloride.

10.1021/bi0255266 CCC: $22.00 
Published on Web 03/28/2002

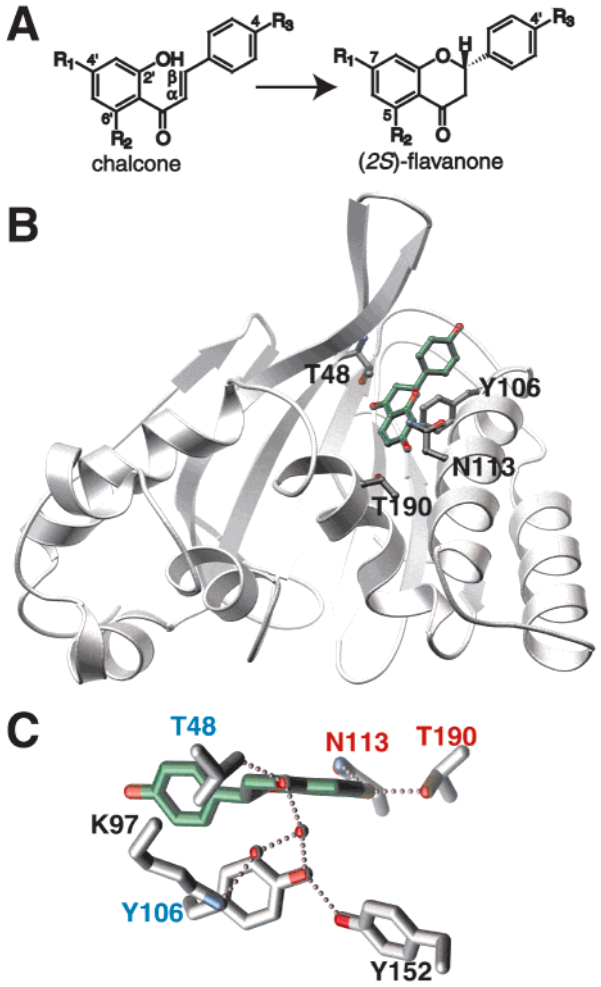


FIGURE 1: CHI reaction and active site. (A) CHI cyclizes 4,2′,4′,6′-tetrahydroxychalcone ($R_1$, $R_2$, $R_3$ = OH), 4,2′,4′-trihydroxychalcone ($R_1$, $R_3$ = OH, $R_2$ = H), 2′,4′-dihydroxychalcone ($R_1$ = OH, $R_2$, $R_3$ = H), and 4,2′-dihydroxychalcone ($R_1$, $R_2$ = H, $R_3$ = OH) into 5,7,4′-trihydroxyflavanone ($R_1$, $R_2$, $R_3$ = OH), 7,4′-dihydroxyflavanone ($R_1$, $R_3$ = OH, $R_2$ = H), 7-hydroxyflavanone ($R_1$ = OH, $R_2$, $R_3$ = H), and 4′-hydroxyflavanone ($R_1$, $R_2$ = H, $R_3$ = OH), respectively. Note that the 4′-hydroxyl group of each substrate becomes the 7-hydroxyl group of the product. (B) Ribbon diagram of CHI showing the location of bound 7,4′-dihydroxyflavanone at the active site. (C) View of the active site hydrogen bond network. Water molecules are shown as red spheres. Dotted lines (rose) indicate hydrogen bonds. The conserved residues of the hydrogen bond network are noted in blue. The residues that hydrogen bond with the flavanone 7-hydroxyl group are noted in red. Figure prepared with MOLSCRIPT (*29*) and rendered with POV-Ray (*30*).

intramolecular cyclization reaction leading to (*S*)-flavanones by precisely positioning a reactive substrate conformer in a preorganized active site.

In the CHI active site, the bound flavanone interacts with the enzyme through complementary van der Waals contacts and two sets of hydrogen bonds (Figure 1C). The extensive hydrogen bond network located at the bottom of the binding cleft contacts the ketone oxygen of the bound flavanone through a water-mediated interaction. Of the five amino acids (Thr48, Ala49, Lys97, Tyr106, and Tyr152) contributing to this network, Thr48 and Tyr106 are conserved in all CHIs (*7*). Preliminary studies suggest that Tyr106 contributes to stabilization of the charged transition state that forms as the cyclization reaction proceeds (*7*). The contribution of Thr48 to catalytic rate enhancement is unresolved, since the crystal structures of several CHI·flavanone complexes reveal two alternate conformations of the side-chain alcohol moiety (*7*, *8*). Asn113 and Thr190 contribute a second set of hydrogen bonds to the flavanone 7-hydroxyl group.

Our goal is to evaluate the contribution of these hydrogen bonds to the reaction mechanism of CHI. Comparisons of the steady-state kinetic parameters, pH−rate profiles, solvent kinetic isotope effects, and solvent viscosity effects on the reactions catalyzed by wild-type CHI and the T48A, T48S, Y106F, N113A, and T190A mutants elucidate roles for both sets of hydrogen bonds in the reaction mechanism of CHI. Finally, the X-ray crystal structures of the T48A and Y106F mutants support the hypothesis that the kinetic effects result from the loss of key hydrogen bonds at the CHI active site.

## EXPERIMENTAL PROCEDURES

*Materials.* All oligonucleotides were synthesized by Operon, Inc. The QuikChange polymerase chain reaction (PCR)-based site-directed mutagenesis kit was purchased from Stratagene. $Ni^{2+}$-NTA was bought from Qiagen. Benzamidine-Sepharose and the Superdex-75 FPLC column were obtained from Amersham Biosciences, Inc. Deuterium oxide, sodium deuterioxide, and deuterium chloride were ordered from Aldrich. Thrombin was purchased from Sigma. 4,2′,4′-Trihydroxychalcone, 2′,4′-dihydroxychalcone, and 4,2′-dihydroxychalcone were bought from Indofine.

*Expression Vector Construction and Site-Directed Mutagenesis.* The CHI T48A, T48S, Y106F, N113A, and T190A mutants were constructed using the QuikChange PCR method with the following pairs of primers (mutated codons are underlined): T48A and T48S [5′-dGGAAACTTCATCAAGTTC(T/G)CTGCCATAGGTGTTTATTTGG-3′ and 5′-dCCAAATAAACACCTATGGCAG(A/C)GAACTTGATGAAGTTTCC-3′]; Y106F [5′-dGGGAATTGAGTGGTCCTGAGTTCTCAAGGAAGGTTATGG-3′ and 5′-dCCATAACCTTCCTTGAGAACTCAGGACCACTCAATTCCC-3′]; N113A [5′-dGGAAGGTTATGGAGGCCTGTGTGGCACACTTGAAATCAGTTGG-3′ and 5′-dCCAACTGATTTCAAGTGTGCCACACAGGCCTCCATAACCTTCC-3′]; T190A [5′-dGCATTCAGCAGTGTTGGAGGCTATGATCGGCGAGCACG-3′ and 5′-dCGTGCTCGCCGATCATAGCCTCCAACACTGCTGAATGC-3′]. Automated nucleotide sequencing confirmed the fidelity of the PCR products (Salk Institute DNA sequencing facility). The resulting mutant cDNAs were subcloned into the pHIS8 expression vector (*9*).

*Protein Expression and Purification.* Wild-type and mutant pHIS8-CHI constructs were transformed into *E. coli* BL21-(DE3) and expressed as described previously (*8*). All recombinant proteins were purified to homogeneity using $Ni^{2+}$-affinity chromatography, benzamidine-Sepharose chromatography, and gel filtration chromatography on a Superdex-75 column (*8*).

*Kinetic Measurements.* The standard CHI assay was performed at 25 °C in a 0.5 mL reaction volume containing 50 mM HEPES (pH 7.5) and 5% (v/v) ethanol as cosolvent (*10*). Measurement of initial velocities used the standard assay system with varied concentrations of either 4,2′,4′,6′-tetrahydroxychalcone (10−200 $\mu$M), 4,2′,4′-trihydroxychalcone (2−75 $\mu$M), 2′,4′-dihydroxychalcone (2−50 $\mu$M), or 4,2′-dihydroxychalcone (2−50 $\mu$M). Maximum substrate

concentrations were limited by compound solubility. All assays using 4,2′,4′,6′-tetrahydroxychalcone as a substrate were corrected for the background reaction rate. Individual saturation curves were fitted to the Michaelis−Menten equation using Kaleidagraph (Synergy Software). Determination of pH−rate profiles and examination of solvent viscosity effects for mutant CHI enzymes were performed as previously described (*8*). The relative solvent viscosity ($\eta^{rel}$) was determined by comparison to the buffer conditions without sucrose using an Ostwald viscometer (*8*). Solvent kinetic isotope effects on $k_{cat}$ and $K_m$ using 4,2′,4′-trihydroxychalcone as a substrate were measured by direct comparison of initial velocities as in the standard assay described above. HEPES reaction buffer was prepared in $D_2O$, and the pH was adjusted with NaOD or DCl to the appropriate pD, where pD = pH + 0.4, to correct for the isotope effect on the response of the glass electrode. The effects on $k_{cat}$ and $K_m$ due to $D_2O$ are expressed using the notation of Northrop (*11*) in which $^{D}V = k_{H_2O}/k_{D_2O}$ and $^{D}V/K = (k_{cat}/K_m)_{H_2O}/(k_{cat}/K_m)_{D_2O}$.

*Structure of the CHI Y106F Mutant.* Crystals of the CHI Y106F mutant grew at 4 °C using the hanging-drop vapor diffusion method from a 2 $\mu$L drop containing a 1:1 mixture of protein and crystallization buffer [25% glycerol (v/v), 2.0 M ammonium sulfate, and 0.1 M TRIS−HCl, pH 8.0] in space group $P6_522$ ($a = b = 89.56$ Å; $c = 351.66$ Å) with two molecules per asymmetric unit. Prior to data collection, crystals were soaked in mother liquor containing 2 mM 4,2′,4′-trihydroxychalcone; however, color change of the drop from yellow to clear indicated formation of 7,4′-dihydroxyflavanone in the crystal. Diffraction data were collected at 105 K from a single crystal on beamline 9-2 of the Stanford Synchrotron Radiation Laboratory (SSRL 9-2) using a Quantum 4 CCD detector. Data reduction was performed with DENZO/SCALEPACK (*12*). The structure was solved by molecular replacement with CNS (*13*) using a model of the apoenzyme structure with an alanine in place of Tyr106. After rigid-body refinement, the $R_{cryst}$ and $R_{free}$ values were 33.8% and 34.9%, respectively, and electron density corresponding to Phe106 was visible in each monomer. In addition, electron density resembling 7,4′-dihydroxyflavanone was observed in monomer A and modeled as such. Strict noncrystallographic symmetry (NCS) was used during the initial round of simulated annealing, positional, and *B*-factor refinement. In subsequent rounds of conjugate gradient minimization, *B*-factor refinement, and manual rebuilding in O (*14*), the NCS constraints were relaxed for residues at the N- and C-termini, the active site, and residues 35−50 (the $\beta$-strand stalk at the top of the structure). In the final rounds of refinement and model building, the NCS constraints were released with the *R*-factors converging to those listed in Table 1. The final model includes residues 2−222 of monomer A, residues 3−39 and 45−217 of monomer B, 101 waters, 4 sulfates, and 1 7,4′-dihydroxyflavanone molecule (monomer A). Atomic coordinates and structure factors for the CHI Y106F mutant have been deposited in the Protein DataBank as 1JX0.

*Structure of the CHI T48A Mutant.* Crystals of CHI T48A mutant were obtained in conditions similar to those described for wild-type CHI [25% glycerol (v/v), 2.2 M ammonium sulfate, and 0.1 M HEPES, pH 7.5] and grew in space group $P6_5$ ($a = b = 90.94$ Å; $c = 349.99$ Å) with six molecules per asymmetric unit and a solvent content of 65%. Prior to data collection, crystals were soaked in mother liquor containing 2 mM 4,2′,4′-trihydroxychalcone. Diffraction data were collected at 105 K from a single crystal on beamline SSRL 9-1 using a 34.5 cm MAR imaging plate detector and were processed as described previously. The three-dimensional structure of the T48A mutant was solved by molecular replacement using CNS and the CHI apoenzyme structure with an alanine in place of Thr48 as the search model. Rotation and translation searches identified six solutions that packed well in the asymmetric unit. After rigid-body refinement in CNS, the $R_{cryst}$ and $R_{free}$ values were 32.7% and 37.5%, respectively. Strict noncrystallographic symmetry (NCS) was used for the initial round of simulated annealing, positional, and *B*-factor refinement. In the next round of conjugate gradient minimization, *B*-factor refinement, and manual rebuilding in O, the NCS constraints were relaxed for residues at the N- and C-termini, the active site, and residues 35−50. During subsequent rounds of refinement and model building, the NCS constraints were released to reflect differences between the six monomers with the *R*-factors converging to those listed in Table 1. The overall structure of each monomer is similar to each other with rms deviations of matching $C_\alpha$ atoms of 0.34−0.66 Å. Although the crystals were soaked with 4,2′,4′-trihydroxychalcone, weak electron density for 7,4′-dihydroxyflavanone was observed only in monomer C of the asymmetric unit and was modeled as such. The final model includes residues 3−40 and 43−222 of monomer A, residues 4−220 of monomer B, residues 4−215 of monomer C, residues 2−39 and 46−222 of monomer D, residues 3−38 and 44−220 of monomer E, residues 5−38 and 44−215 of monomer F, 3 sulfates, 518 waters, and 1 7,4′-dihydroxyflavanone molecule (monomer C). Atomic coordinates and structure factors for the CHI T48A mutant have been deposited in the Protein DataBank as 1JX1.

Table 1: Crystallographic Data and Refinement Statistics for the CHI T48A and Y106F Mutants

| | T48A | Y106F |
|---|---|---|
| wavelength (Å) | 0.970 | 1.008 |
| resolution range (Å) | 79.1−2.30 | 58.0−2.85 |
| total observations | 326009 | 261225 |
| unique reflections | 63669 | 19000 |
| completeness[a] (%) | 88.1 (70.3) | 96.4 (96.1) |
| $I/\sigma$[a] | 12.0 (1.3) | 19.9 (2.7) |
| $R_{sym}$[a,b] (%) | 6.8 (48.6) | 6.4 (51.6) |
| $R_{cryst}$[c]/$R_{free}$[d] (%) | 23.0/28.6 | 26.3/28.4 |
| protein atoms | 9703 | 3193 |
| water molecules | 518 | 101 |
| flavanone atoms | 19 | 19 |
| sulfate atoms | 15 | 20 |
| rmsd lengths (Å) | 0.008 | 0.012 |
| rmsd angles (deg) | 1.4 | 1.7 |
| protein avg *B*-factor (Å$^2$) | 43.9 | 68.6 |
| water avg *B*-factor (Å$^2$) | 48.4 | 69.5 |
| ligand avg *B*-factor (Å$^2$) | 83.0 | 104 |

[a] Numbers in parentheses are for the highest resolution shell. [b] $R_{sym} = \sum|I_h - \langle I_h \rangle|/\sum I_h$, where $\langle I_h \rangle$ is the average intensity over symmetry-equivalent reflections. [c] *R*-factor $= \sum|F_{obs} - F_{calc}|/\sum F_{obs}$, where summation is over the data used for refinement. [d] $R_{free}$-factor was calculated using 5% of data excluded from refinement.

## RESULTS

*Expression and Purification of Recombinant Proteins.* Recombinant wild-type and mutant CHIs were overexpressed

Table 2: Steady-State Kinetic Parameters of Wild-Type and Mutant CHI[a]

| | 4,2′,4′,6′-tetrahydroxychalcone | | | 4,2′,4′-trihydroxychalcone | | |
|---|---|---|---|---|---|---|
| | $k_{cat}$ ($min^{-1}$) | $K_m$ ($\mu M$) | $k_{cat}/K_m$ ($M^{-1}$ $s^{-1}$) | $k_{cat}$ ($min^{-1}$) | $K_m$ ($\mu M$) | $k_{cat}/K_m$ ($M^{-1}$ $s^{-1}$) |
| CHI[b] | 11180 ± 1380 | 112 ± 28 | 1660000 | 2250 ± 165 | 8.4 ± 2.0 | 4460000 |
| T48S | 12900 ± 6500 | 516 ± 341 | 420000 | 830 ± 86 | 21.3 ± 4.1 | 650000 |
| T48A | 88.6 ± 13 | 182 ± 91 | 8110 | 1.45 ± 0.11 | 18.9 ± 3.2 | 1280 |
| Y106F | 396 ± 93 | 168 ± 70 | 39300 | 75.2 ± 6.4 | 12.4 ± 2.4 | 101000 |
| N113A | 783 ± 154 | 449 ± 79 | 29100 | 304 ± 33 | 24.3 ± 3.8 | 209000 |
| T190A | 506 ± 160 | 263 ± 132 | 32100 | 379 ± 54 | 19.8 ± 2.7 | 319000 |
| | 2′,4′-dihydroxychalcone | | | 4,2′-dihydroxychalcone | | |
| | $k_{cat}$ ($min^{-1}$) | $K_m$ ($\mu M$) | $k_{cat}/K_m$ ($M^{-1}$ $s^{-1}$) | $k_{cat}$ ($min^{-1}$) | $K_m$ ($\mu M$) | $k_{cat}/K_m$ ($M^{-1}$ $s^{-1}$) |
| CHI[b] | 755 ± 33 | 22.7 ± 4.2 | 554000 | 92.1 ± 20.5 | 42.5 ± 5.3 | 36100 |
| T48S | 519 ± 63 | 41.0 ± 4.2 | 197000 | 54.1 ± 9.7 | 56.0 ± 4.6 | 16,100 |
| T48A | 1.07 ± 0.06 | 15.0 ± 2.2 | 1190 | 0.28 ± 0.05 | 46.4 ± 7.6 | 101 |
| Y106F | 34.1 ± 3.1 | 34.6 ± 5.9 | 16400 | 53.5 ± 8.4 | 46.9 ± 7.0 | 19000 |
| N113A | 284 ± 42 | 17.4 ± 3.6 | 272000 | 343 ± 58 | 52.5 ± 10.6 | 109000 |
| T190A | 176 ± 20 | 19.2 ± 2.5 | 153000 | 225 ± 47 | 55.9 ± 8.4 | 67100 |

[a] Reactions were performed in HEPES buffer (pH 7.5) as described under Experimental Procedures. All $k_{cat}$ and $K_m$ values are expressed as mean ± SE for $n = 3$. [b] Values for wild-type CHI were previously determined (*8*).

in *E. coli* as octahistidine-tagged proteins and purified to homogeneity using $Ni^{2+}$-affinity and gel filtration chromatography. The His-tag was removed prior to gel filtration by thrombin digestion. All CHI forms migrated on SDS−PAGE gels with a molecular mass of 24 kDa and eluted from the gel filtration column as monomers of approximately the same molecular mass (not shown). Yields were typically 7−10 mg of pure protein per liter of *E. coli*.

*Steady-State Kinetic Parameters of the CHI Mutants.* The first set of mutations (T48S, T48A, and Y106F) focus on the hydrogen bond network located at the bottom of the active site cleft. The second set of mutations (N113A and T190A) target residues that potentially interact with the chalcone 4′-hydroxyl group (Figure 1C). The steady-state kinetic constants of wild-type and mutant CHI for 4,2′,4′,6′-tetrahydroxychalcone, 4,2′,4′-trihydroxychalcone, 2′,4′-dihydroxychalcone, and 4,2′-dihydroxychalcone are summarized in Table 2.

Of the mutations to the hydrogen bond network, substitution of Thr48 by serine yields the smallest changes in the measured kinetic constants with all four chalcones examined. The Y106F and T48A mutants exhibit the largest changes in the $k_{cat}$ and $k_{cat}/K_m$ values for each substrate. Mutation of Tyr106 to a phenylalanine reduces the $k_{cat}$ values nearly 30-fold for both 4,2′,4′,6′-tetrahydroxychalcone and 4,2′,4′-trihydroxychalcone, 22-fold for 2′,4′-dihydroxychalcone, and 2-fold for 4,2′-dihydroxychalcone with minor variations in the $K_m$ values. Replacement of Thr48 with an alanine causes 130-, 1550-, 700-, and 330-fold reductions in $k_{cat}$ with 4,2′,4′,6′-tetrahydroxychalcone, 4,2′,4′-trihydroxychalcone, 2′,4′-dihydroxychalcone, and 4,2′-dihydroxychalcone, respectively, with less than 2-fold differences in $K_m$ for the same substrates.

Mutation of either Asn113 or Thr190 to an alanine eliminates a potential hydrogen bond to the substrate 4′-hydroxyl group. The N113A mutation reduces the $k_{cat}$ values for 4,2′,4′,6′-tetrahydroxychalcone, 4,2′,4′-trihydroxychalcone, and 2′,4′-dihydroxychalcone by 14-, 7-, and 3-fold, respectively. Likewise, the T190A mutant exhibits 22-, 6-, and 4-fold reductions in the $k_{cat}$ values with 4,2′,4′,6′-tetrahydroxychalcone, 4,2′,4′-trihydroxychalcone, and 2′,4′-dihydroxychalcone, respectively. Both mutants display 2−4-fold changes in $K_m$ for these chalcones. With 4,2′-dihydroxychalcone as a substrate, the calculated $k_{cat}$ values and the corresponding $k_{cat}/K_m$ values of the N113A and T190A mutants increase 2−3-fold compared to wild-type CHI. Since the determined $K_m$ values are at the limit of solubility for this substrate, these values are estimates of the actual steady-state parameters.

*Effect of CHI Mutations on the pH-Dependence of 4,2′,4′-Trihydroxychalcone Cyclization.* To evaluate the contribution of each set of hydrogen bonds toward altering the p$K_a$ of the CHI-catalyzed cyclization reaction, the pH-dependence on $k_{cat}$ and $k_{cat}/K_m$ of the T48A, T48S, Y106F, N113A, and T190A mutants was examined using 4,2′,4′-trihydroxychalcone as a substrate (Figure 2 and Table 3). Since saturation of wild-type and mutant CHI occurs with 4,2′,4′-trihydroxychalcone, the solvent viscosity and solvent kinetic isotope effect experiments described below employ this substrate. None of the mutations significantly alter the protonation state of either free substrate or free enzyme, since the p$K_a$ values for $k_{cat}/K_m$ of each mutant enzyme are similar to that of wild-type CHI. Each mutation shifts the p$K_a$ of $k_{cat}$ closer to the p$K_a$ values of $k_{cat}/K_m$, suggesting that elimination of individual hydrogen bond interactions partly affects the ionization state of the enzyme·substrate complex.

*Solvent Viscosity Effects on 4,2′,4′-Trihydroxychalcone Cyclization Catalyzed by Mutant CHI.* Previously, we established that the cyclization of 4,2′,4′-trihydroxychalcone catalyzed by wild-type CHI is a diffusion-controlled reaction (*8*). Since diffusion of a small molecule is inversely proportional to the relative viscosity of bulk solvent, increasing the concentration of microviscogens, like sucrose or glycerol, can affect the diffusion of substrates and products and provide an estimate of the diffusional control of a bimolecular reaction. Here we examine the effect of active site mutants on the rate-limiting step of the reaction mechanism (eq 1) by perturbing the steady-state kinetic mechanism using solvent viscosity experiments (*15*−*20*).

$$E + S \underset{k_{-1}}{\overset{k_1}{\rightleftharpoons}} ES \overset{k_2}{\rightleftharpoons} EP \overset{k_3}{\rightleftharpoons} E + P \qquad (1)$$

If this kinetic mechanism is diffusion-controlled, changes

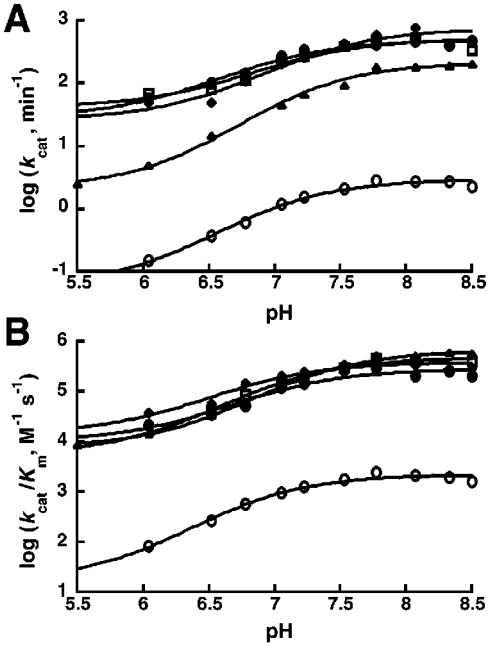


FIGURE 2: pH-dependence of 4,2′,4′-trihydroxychalcone cyclization catalyzed by mutant CHI. (A) log($k_{cat}$) versus pH. (B) log($k_{cat}/K_m$) versus pH. The pH-dependence of the T48S (circles), T48A (open circles), Y106F (triangles), N113A (diamonds), and T190A (open squares) mutants was determined using a triple buffer system as described previously (*8*). Each data point represents the mean of three measurements with standard errors of 5−10%.

Table 3: p$K_a$ Values from pH Profiles for $k_{cat}$ and $k_{cat}/K_m$ for Mutant CHI with 4,2′,4′-Trihydroxychalcone[a]

| | $k_{cat}$ (min$^{-1}$) | | $k_{cat}/K_m$ (M$^{-1}$ s$^{-1}$) | |
|---|---|---|---|---|
| | p$K_a$ | $Y_{max}$[b] | p$K_a$ | $Y_{max}$[b] |
| CHI[c] | 6.20 ± 0.06 | 6370 ± 36 | 6.70 ± 0.09 | 3390000 ± 22800 |
| T48S | 6.58 ± 0.10 | 500 ± 5 | 6.66 ± 0.18 | 285000 ± 3260 |
| T48A | 6.56 ± 0.08 | 2.99 ± 0.18 | 6.47 ± 0.12 | 2240 ± 62 |
| Y106F | 6.72 ± 0.06 | 219 ± 4 | 6.83 ± 0.04 | 575000 ± 2490 |
| N113A | 6.91 ± 0.16 | 767 ± 22 | 6.49 ± 0.18 | 392000 ± 3810 |
| T190A | 6.82 ± 0.21 | 524 ± 28 | 6.59 ± 0.17 | 478000 ± 3280 |

[a] Determination of steady-state kinetic parameters over a pH range (5.5−8.5) was performed using a triple buffer system as described previously (*8*). [b] pH-independent values for $k_{cat}$ and $k_{cat}/K_m$ are expressed in units of min$^{-1}$ and M$^{-1}$ s$^{-1}$, respectively. [c] Wild-type CHI values were previously determined (*8*).

in microviscosity affect $k_1$ and $k_{-1}$, but not $k_2$ (*19*). The ratio of $K_m/V_{max}$ will depend on the relative viscosity ($\eta^{rel}$) of the solution according to eq 2 (*15*, *17*); and if the rate of product dissociation is kinetically limiting, then $1/V_{max}$ versus relative viscosity ($\eta^{rel}$) will vary as eq 3 (*20*).

$$K_m/V_{max} = \eta^{rel}/k_1 + k_{-1}/k_1k_2 \quad (2)$$

$$1/V_{max} = \eta^{rel}/k_3 - 1/k_2 \quad (3)$$

Each CHI mutant behaves differently as the solvent viscosity is varied (Figure 3A). Mutation of either Tyr106 to a phenylalanine or Thr48 to an alanine yields enzymes exhibiting a cleanly rate-limiting chemical step, since increasing the solvent viscosity of the reaction solution does not alter the measured kinetic constants (*21*). The T48S, N113A, and T190A mutants, like wild-type CHI, display a kinetic dependence only when the microviscosity of the

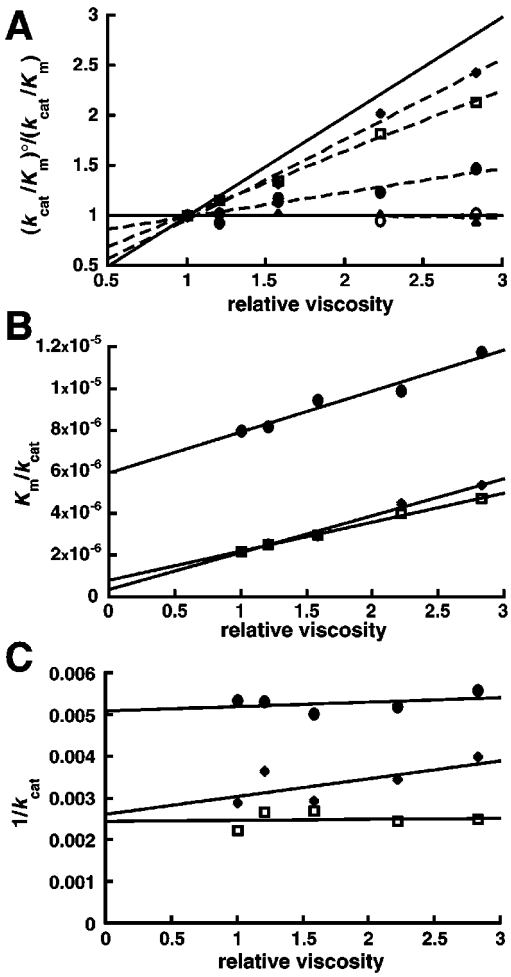


FIGURE 3: Solvent viscosity effect on 4,2′,4′-trihydroxychalcone cyclization catalyzed by mutant CHI. (A) Plot of the relative second-order rate constant as a function of relative viscosity ($\eta^{rel}$) for the T48S (circles), T48A (open circles), Y106F (triangles), N113A (diamonds), and T190A (open squares) mutants. Each data point represents the mean of three measurements with standard errors of 5−10%. The superscript 'o' denotes the absence of viscogen. The upper solid line (slope = 1) represents the limit of a diffusion-controlled reaction, and the lower solid line (slope = 0) represents a reaction without any viscosity effect. The dashed lines from top to bottom are fits of the T190A, N113A, T48S, Y106F, and T48A data, respectively. (B) Plot of $K_m/k_{cat}$ versus relative viscosity for the T48S (circles), N113A (diamonds), and T190A (open squares) mutants. (C) Plot of $1/k_{cat}$ versus relative viscosity for the T48S (circles), N113A (diamonds), and T190A (open squares) mutants.

solution is varied. High molecular weight polymers, like Ficoll, alter the macroviscogenic properties of solvent without affecting the diffusion of small molecules in solution. To verify that the observed effects result solely from changes in microviscosity, the T48S, N113A, and T190A mutants were assayed in the presence of Ficoll 400 ($\eta^{rel}$ = 2.2), a macroviscogen, without any effect.

Quantitative analysis of the T48S, N113A, and T190A solvent viscosity experiments provides estimates of the microscopic rate constants for the CHI reaction mechanism (*15*, *17*, *20*). A plot of $K_m/k_{cat}$ versus relative viscosity yields values for $k_1$ and the partition ratio ($k_{-1}/k_2$) (Figure 3B and Table 4). Likewise, a plot of $1/k_{cat}$ versus relative viscosity provides the values of $k_2$ and $k_3$ (Figure 3C and Table 4) and indicates that product dissociation ($k_3$) is not rate-limiting for either the T48S, N113A, or T190A mutants. The quotient

Table 4: Values of Kinetic Constants Derived from Solvent Viscosity Effects

| | $k_1$ ($M^{-1}$ $s^{-1}$)[a] | $k_{-1}$ ($min^{-1}$)[b] | $k_2$ ($min^{-1}$)[c] | $k_3$ ($min^{-1}$)[d] |
|---|---|---|---|---|
| CHI[e] | 5210000 | 1330 | 2736 | 33700 |
| T48S | 508000 | 2717 | 961 | 8760 |
| N113A | 460000 | 81 | 382 | 2282 |
| T190A | 417000 | 319 | 406 | 35200 |

[a] $k_1$, determined from slope of fit (eq 2) in Figure 3B (*15, 17*). [b] $k_{-1}$, determined from intercept of fit (eq 2) in Figure 3B (*15, 17*). [c] $k_2$, determined from intercept of fit (eq 3) in Figure 3C (*20*). [d] $k_3$, determined from slope of fit (eq 3) in Figure 3C (*20*). [e] Rate constants for wild-type CHI were previously determined (*8*).

Table 5: Solvent Isotope Effects for Wild-Type and Mutant CHI with 4,2′,4′-Trihydroxychalcone[a]

| | $^{D}V$ | $^{D}V/K$ |
|---|---|---|
| CHI | 1.01 ± 0.01 | 1.46 ± 0.09 |
| T48S | 1.06 ± 0.03 | 1.35 ± 0.01 |
| T48A | 1.26 ± 0.01 | 1.08 ± 0.04 |
| Y106F | 1.32 ± 0.04 | 1.08 ± 0.06 |
| N113A | 1.00 ± 0.06 | 1.27 ± 0.02 |
| T190A | 0.99 ± 0.01 | 1.49 ± 0.03 |

[a] All values are mean ± SE for $n = 3$.

of $k_{cat}/K_m$ and $k_1$ demonstrates that the reactions of the T48S, N113A, and T190A mutants are 78%, 45%, and 77% diffusion-controlled, respectively.

*Effect of $D_2O$ on 4,2′,4′-Trihydroxychalcone Cyclization Catalyzed by Wild-Type and Mutant CHI.* Solvent kinetic isotope effects were determined using 4,2′,4′-trihydroxychalcone as a substrate for wild-type CHI and the T48A, T48S, Y106F, N113A, and T190A mutants (Table 5). Wild-type CHI and the T48S, N113A, and T190A mutants exhibit $D_2O$ effects on $k_{cat}/K_m$, while there is a substantial loss of the $D_2O$ effect for the T48A and Y106F mutants. Moreover, wild-type CHI and the T48S, N113A, and T190A mutants do not display solvent kinetic isotope effects on $k_{cat}$, while the T48A and Y106F mutants again behave in an opposite fashion, showing measurable $D_2O$ effects on $k_{cat}$.

*Structures of the T48A and Y106F Mutants.* Since the T48A and Y106F mutations had the largest effect on the steady-state kinetic parameters of CHI and precipitated a change in the rate-limiting step compared to wild-type CHI and the other mutants, the X-ray crystal structures of these two CHI mutants were determined to evaluate potential structural alterations at the CHI active site. The overall three-dimensional structures of the T48A and Y106F mutants are similar to those of the wild-type CHI·7,4′-dihydroxyflavanone complex (*8*) with 0.41 and 0.38 Å rms deviations of the $C_\alpha$ atoms, respectively.

The 2.3 Å resolution crystal structure of the T48A mutant reveals that substitution of an alanine for Thr48 causes no significant structural variations among the residues of the CHI active site (Figure 4A). Although this mutation abrogates formation of the hydrogen bond between the side-chain hydroxyl group of Thr48 and the flavanone ketone oxygen, the flavanone observed in monomer C is positioned as in the wild-type CHI·7,4′-dihydroxyflavanone complex (*8*). The major difference between the wild-type and T48A complexes is that both active site water molecules are missing in the structure of the T48A·7,4′-dihydroxyflavanone complex (Figure 4B,C). However, in the other T48A monomers of the asymmetric unit which lack the flavanone at the active site, the water molecule that forms a hydrogen bond with Lys97 remains in position, but no electron density corresponding to the second water molecule that interacts with Tyr106 and the flavanone ketone oxygen is discernible.

The 2.85 Å resolution crystal structure of the CHI Y106F mutant exhibits alterations in the positions of several active site residues (Figure 4D), and no electron density corresponding to the active site water molecules is discernible in the Y106F mutant. Although accurate depiction of the active site water network is problematic given the resolution of the Y106F structure, the three-dimensional structure of this mutant confirms that mutation of Tyr106 to a phenylalanine eliminates a hydrogen bond with the water molecule interacting with the flavanone ketone oxygen without perturbing the active site architecture. In addition, the position of 7,4′-dihydroxyflavanone in the active site of the Y106F mutant is nearly identical to the position first observed in the structure of wild-type CHI complexed with the same flavanone (*8*). In the structure of the Y106F mutant, Thr48 adopts the conformation originally observed in wild-type CHI and the CHI·naringenin complex (*7*). In these instances, the side-chain hydroxyl group points toward the water network and not toward the ketone oxygen of the bound flavanone. Interestingly, the δ-guanido moiety of Arg36 shifts position in the Y106F mutant structure following disruption of the electrostatic interaction between this basic side-chain and Asp200.

## DISCUSSION

We have examined the contribution of two sets of hydrogen bonds to the intramolecular cyclization reaction catalyzed by CHI using steady-state kinetic analysis of a series of point mutants. These functional studies and the three-dimensional structures of the T48A and Y106F mutants elucidate the contribution of hydrogen bonds to the reaction mechanism of CHI.

*Hydrogen Bonding with the Chalcone 4′-Hydroxyl Group during Catalytic Turnover.* The three-dimensional structures of wild-type CHI complexed with naringenin (5,7,4′-trihydroxyflavanone), 7,4′-dihydroxyflavanone, and 7-hydroxyflavanone indicate that Asn113 and Thr190 form hydrogen bonds with the 7-hydroxyl group of the flavanone product (*7, 8*). Although the corresponding 4′-hydroxyl group of a chalcone substrate is not formally involved in the intramolecular Michael addition, mutation of either Asn113 or Thr190 to an alanine has a large effect on $k_{cat}$ with each chalcone tested. Such effects indicate that these mutations eliminate potential interactions with the transition state of the reaction. Likewise, the pH-dependence of the N113A and T190A mutants supports this assertion. Experiments examining the pH-dependence of the nonenzymatic and CHI-catalyzed cyclization of chalcones into flavanones demonstrate that deprotonation of the 2′-hydroxyl group to yield a reactive oxyanion readily occurs in solution (*8, 22*−*24*). The observed effect of the N113A and T190A mutations on the $pK_a$ of $k_{cat}$ and not $k_{cat}/K_m$ in the cyclization of 4,2′,4′-trihydroxychalcone shows that interaction between these residues and the substrate slightly polarizes the enzyme·substrate complex during the reaction.

Previous studies show that the cyclization reaction catalyzed by wild-type CHI is approximately 90% diffusion-

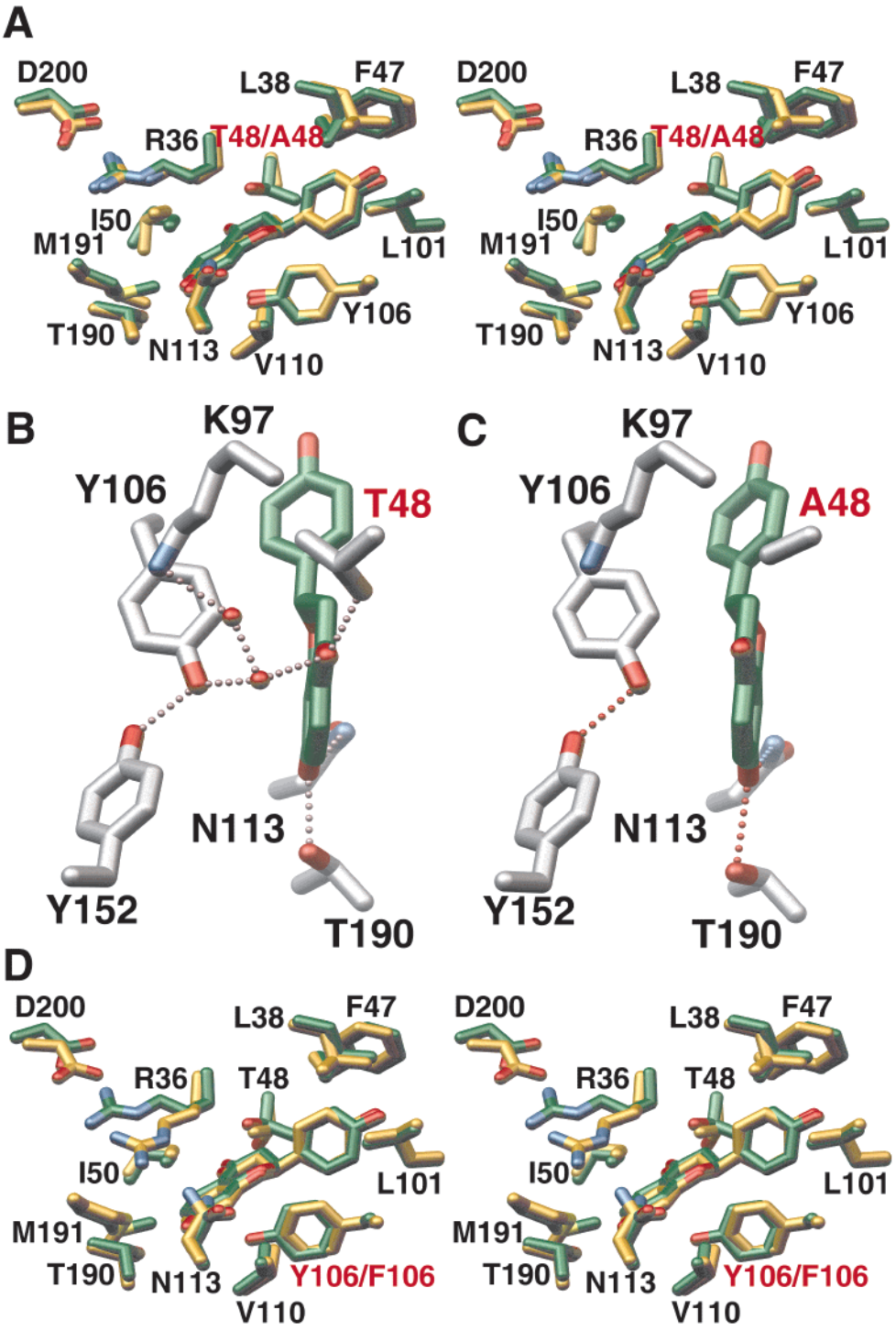


FIGURE 4: Active site comparison between wild-type CHI and the T48A and Y106F mutants. (A) Overlay of the active sites of wild-type CHI complexed with 7,4′-dihydroxyflavanone (green, ref *8*) and the T48A mutant (gold). (B) The active site hydrogen bond network of the wild-type CHI·7,4′-dihydroxyflavanone complex (*8*). (C) The active site hydrogen bond network of the T48A·7,4′-dihydroxyflavanone complex. (D) Overlay of the active sites of wild-type CHI complexed with 7,4′-dihydroxyflavanone (green, ref *8*) and the Y106F mutant (gold). Figure prepared with MOLSCRIPT (*31*) and rendered with POV-Ray (*32*).

controlled (*8*). Although the N113A and T190A mutants exhibit solvent viscosity effects similar to wild-type CHI, the reduction in $k_{cat}$ for each mutant suggests that a chemical step has become more rate-limiting, as reflected in the partially diffusion-controlled reactions of the N113A and T190A mutants (45% and 77% diffusion-controlled, respectively). However, the observed solvent kinetic isotope effects on *V*/*K* and not *V* for wild-type CHI and the N113A and T190A mutants indicate that the contribution of a chemical step involving proton transfer to the overall reaction rate is negligible. The observed effect on *V*/*K* for wild-type CHI and these two mutants likely results from the 23% higher viscosity of $D_2O$ over $H_2O$ (*25*).

The overall effect of the N113A and T190A mutations on turnover rate may derive from the loss in polarization of the enzyme·substrate complex and/or from alterations in how the chalcone binds at the active site. The percentages of catalytically productive collisions offer support for the latter

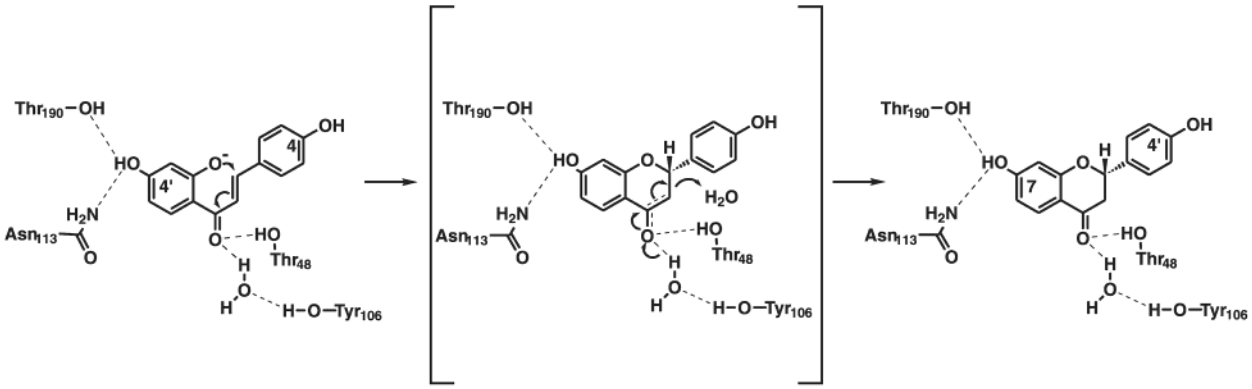


FIGURE 5: Hydrogen bonds in the reaction mechanism of CHI. The roles of Thr48, Tyr106, Asn113, and Thr190 in the reaction mechanism are shown for the cyclization of 4,2′,4′-trihydroxychalcone into 7,4′-dihydroxyflavanone. Note that the substrate 4′-hydroxyl group becomes the 7-hydroxyl group of the product.

hypothesis. The theoretical diffusion limit for a bimolecular reaction is $10^8$−$10^{10}$ $M^{-1}$ $s^{-1}$. At pH 7.5, roughly 5% ($k_{cat}/K_m$ divided by $10^8$ $M^{-1}$ $s^{-1}$) of the diffusional collisions between wild-type CHI and 4,2′,4′-trihydroxychalcone are catalytically productive (*8*). With the N113A and T190A mutants, less than 0.03% of collisions between substrate and enzyme are productive. Moreover, the effect of these mutations on the substrate disassociation rate ($k_{-1}$) and the rate of product release ($k_3$) indicates that Asn113 and Thr190 contribute differently to binding chalcones and flavanones. These results suggest that Asn113 and Thr190 orient the substrate at the active site and position the reactive 2′-oxyanion of the substrate in proximity to the α,β-unsaturated double bond for the intramolecular cyclization reaction.

*Role of Thr48 and Tyr106 in Catalysis.* Structurally, Thr48 and Tyr106 form part of a hydrogen bond network that includes two water molecules at the bottom of the active site cleft and are strictly conserved in CHIs from other plant species (*7*). The three-dimensional structure of CHI complexed with naringenin and preliminary kinetic characterization of the Y106F mutant suggested that Tyr106 stabilizes a catalytic water molecule, which contacts the chalcone ketone and may act as a general acid in the transient protonation of the enolate intermediate (*7*). Based on the structure of the CHI·naringenin complex, Thr48 appeared to help maintain the structure of the active site water network (*7*). However, subsequent determination of the three-dimensional structures of CHI complexed with 7,4′-dihydroxyflavanone, 7-hydroxyflavanone, and 4′-hydroxyflavanone revealed an alternative conformation of Thr48 that allows the side-chain hydroxyl group to directly interact with the flavanone ketone moiety, suggesting that this residue directly participates in catalysis (*8*).

Comparison of the steady-state kinetic parameters of the T48A, T48S, and Y106F mutants versus wild-type CHI indicates that both Thr48 and Tyr106 facilitate the intramolecular cyclization of chalcones into flavanones. Although substitution of a serine for Thr48 is tolerated, the T48A and Y106F mutants are catalytically impaired. Examination of the effect of these mutations on $k_{cat}$ and $k_{cat}/K_m$ indicates that Thr48 is more important for efficient catalysis than Tyr106. These mutations, like the N113A and T190A mutations, only slightly shift the p$K_a$ of the enzyme·substrate complex. The most dramatic effect of the T48A and Y106F mutants is the change from a diffusion-controlled reaction to a chemically limited one. This is evident from the solvent viscosity experiments in which there is no alteration in kinetic parameters for either mutant.

The effect of $D_2O$ on the steady-state kinetic parameters also corroborates the solvent viscosity experiments. The absence of a solvent kinetic isotope effect on *V*/*K* supports the loss of diffusional control in the reactions catalyzed by the T48A and Y106F mutants and supports the assertion that a chemical step has become rate-limiting. The approximate 1.3-fold decrease in turnover rate for both these mutants in $D_2O$ suggests that a proton transfer step in the reaction mechanism now partially contributes to limiting the reaction rate.

The three-dimensional structures of the T48A and Y106F mutants confirm that the overall positions of residues lining the active site are not rearranged, with the exception of Arg36 in the Y106F structure, as discussed later. Substitution of an alanine for Thr48 does not alter the position of the flavanone in the active site complex, but this mutation may affect the active site water structure. Although no water molecules are observed in the active site of the T48A monomer with 7,4′-dihydroxyflavanone bound, the water molecule that hydrogen bonds to Lys97 is present in other T48A monomers of the asymmetric unit. In none of the six monomers of the asymmetric unit is electron density corresponding to the second water molecule observed. Likewise, in the Y106F mutant structure, no waters are observed at the active site, despite the presence of Thr48 and Lys97, which can interact with the first water molecule. The resolution of the Y106F structure makes an accurate assessment of the active site water structure problematic. Nonetheless, these X-ray crystal structures verify that elimination of key hydrogen bonds from the CHI active site correlates with reductions in the catalytic efficiency of the enzyme either through a loss of direct interactions with the substrate during catalysis and/or by disrupting the active site water network. Given the three-dimensional architecture of the CHI active site, both explanations are likely entwined.

*Reaction Mechanism.* CHI catalyzes the intramolecular cyclization of chalcones into (*S*)-flavanones with a $10^7$-fold rate enhancement over the nonenzymatic cyclization rate (*8*, *10*). The three-dimensional structure of CHI indicated that the active site limits the conformation of the chalcone substrate and brings the reactive centers of the chalcone molecule, i.e., the 2′-oxyanion and an α,β-unsaturated double

bond, into proximity for catalysis (*7*). The experiments presented here provide the first functional evidence that specific hydrogen bond interactions at the CHI active site contribute to catalysis (Figure 5).

Examination of the steady-state kinetics of the N113A and T190A mutants, combined with solvent kinetic isotope effect and solvent viscosity effect experiments, demonstrates the role of the interaction between these two residues and the chalcone 4′-hydroxyl group. While not directly involved at the site of catalysis on the chalcone, these hydrogen bonds likely contribute binding energy to enhance the catalytic rate (*26*−*28*). Likewise, steady-state kinetic experiments and crystallographic examination of the T48A and Y106F mutants confirm the importance of the hydrogen bond network at the bottom of the active site for CHI-catalyzed flavanone formation. Based on previous work (*7*, *8*) and the experiments presented here, we propose that Thr48 directly interacts with the ketone of the chalcone and that Tyr106 stabilizes the catalytic water molecule during transient protonation of the intermediate enolate. Both these interactions stabilize the transition state during the intramolecular cyclization reaction.

Comparison of the amino acid sequences of CHI from other plant species suggests that these enzymes share a common reaction mechanism. Conservation of Thr48, Tyr106, and Asn113 occurs in all CHIs examined to date (*7*). CHIs from legumes have a threonine at position 190, but CHIs from other plants have a serine at this position. Previously, we suggested that this change may explain the difference in substrate specificity between CHI from legumes and other plants (*7*); however, substitution of a serine for Thr190 does not change the substrate specificity or steady-state kinetic parameters of alfalfa CHI using a variety of chalcones (J.M.J. and J.P.N., unpublished observations).

Finally, the observed movement of Arg36 toward the 7,4′-dihydroxyflavanone molecule in the three-dimensional structure of the Y106F mutant suggests that this basic residue may have a role in catalysis. Crystals of this mutant only grew at a higher pH (8.0) than used for previous crystallization experiments, and the change in pH seemingly alters the electrostatic interaction between Arg36 and Asp200. Each of the previous structures of CHI (*7*, *8*) showed that the $\delta$-guanido group of Arg36 and the carboxylate of Asp200 form an electrostatic interaction. In the conformation observed in the Y106F mutant, the positively charged $\delta$-guanido group of Arg36 is in proximity to the aromatic ring of the chalcone substrate bearing the 2′-oxyanion. Currently, we are exploring the potential role of Arg36 in the CHI reaction mechanism.

## ACKNOWLEDGMENT

We thank the Pollard lab for use of their spectrophotometer, E. Dutil and S. Koenig for assistance during data collection at SSRL, and C. Dana (Virginia Tech) for providing a sample of 4,2′,4′,6′-tetrahydroxychalcone for these studies. The SSRL Biotechnology Program is supported by the NIH, National Center for Research Resources, Biomedical Technology Program, and the DOE, Office of Biological and Environmental Research.

## REFERENCES

1. Bohm, B. A. (1998) *Introduction to Flavonoids*, Harcourt, Singapore.
2. DellaPenna, D. (1999) *Science 285*, 375−379.
3. Muir, S. R., Collins, G. J., Robinson, S., Hughes, S., Bovy, A., De Vos, C. H. R., van Tunen, A. J., and Verhoeyen, M. E. (2001) *Nat. Biotechnol. 19*, 470−474.
4. Dixon, R. A., and Steele, C. J. (1999) *Trends Plant Sci. 4*, 394−400.
5. Moustafa, E., and Wong, E. (1967) *Phytochemistry 6*, 625−632.
6. Hahlbrock, K., Zilg, H., and Grisebach, H. (1970) *Eur. J. Biochem. 15*, 13−18.
7. Jez, J. M., Bowman, M. E., Dixon, R. A., and Noel, J. P. (2000) *Nat. Struct. Biol. 7*, 786−791.
8. Jez, J. M., and Noel, J. P. (2002) *J. Biol. Chem. 277*, 1361−1369.
9. Jez, J. M., Ferrer, J.-L., Bowman, M. E., Dixon, R. A., and Noel, J. P. (2000) *Biochemistry 39*, 890−902.
10. Bednar, R. A., and Hadcock, J. R. (1988) *J. Biol. Chem. 263*, 9582−9588.
11. Northrop, D. B. (1981) *Annu. Rev. Biochem. 50*, 103−131.
12. Otwinowski, Z., and Minor, W. (1997) *Methods Enzymol. 276*, 307−326.
13. Brünger, A. T., Adams, P. D., Clore, G. M., DeLano, W. L., Gros, P., Grosse-Kunstleve, R. W., Jiang, J. S., Kuszewski, J., Nilges, M., Pannu, N. S., Read, R. J., Rice, L. M., Simonson, T., and Warren, G. L. (1998) *Acta Crystallogr. D54*, 905−921.
14. Jones, T. A., Zou, J. Y., Cowan, S. W., and Kjeldgaard, M. (1993) *Acta Crystallogr. D49*, 148−157.
15. Loo, S., and Erman, J. E. (1977) *Biochim. Biophys. Acta 481*, 279−282.
16. Dunford, H. B., and Hewson, W. D. (1977) *Biochemistry 16*, 2949−2957.
17. Brouwer, A. C., and Kirsch, J. F. (1982) *Biochemistry 21*, 1302−1307.
18. Blacknow, S. C., Raines, R. T., Lim, W. A., Zamore, P. D., and Knowles, J. R. (1988) *Biochemistry 27*, 1158−1167.
19. Cleland, W. W. (1990) *Enzymes (3rd Ed.) 19*, 99−158.
20. Kurz, L. C., Weitkamp, E., and Frieden, C. (1987) *Biochemistry 26*, 3027−3032.
21. Grace, M. R., Walsh, C. T., and Cole, P. A. (1997) *Biochemistry 36*, 1874−1881.
22. Miles, C. O., and Main, L. (1985) *J. Chem. Soc., Perkin Trans. 2*, 1639−1642.
23. Furlong, J. J. P., and Nudelman, N. S. (1985) *J. Chem. Soc., Perkin Trans. II*, 633−649.
24. Furlong, J. J. P., and Nudelman, N. S. (1988) *J. Chem. Soc., Perkin Trans. II*, 1213−1217.
25. Walsh, C. (1979) in *Enzymatic Reaction Mechanisms*, pp 121−122, W. W. H. Freeman, New York.
26. Leatherbarrow, R. J., Fersht, A. R., and Winter, G. (1985) *Proc. Natl. Acad. Sci. U.S.A. 82*, 7840−7844.
27. Fersht, A. R., Shi, J. P., Knill-Jones, J., Lowe, D. M., Wilkinson, A. J., Blow, D. M., Brick, P., Carter, P., Waye, M. M., and Winter, G. (1985) *Nature 314*, 235−238.
28. Wells, T. C. N., and Fersht, A. R. (1986) *Biochemistry 25*, 1881−1886.
29. Kraulis, P. J. (1991) *J. Appl. Crystallogr. 24*, 946−950.
30. POV-Team (1997) POV-Ray: persistence of vision ray-tracer; www.povray.org.

BI0255266